Toxicology and Applied Pharmacology 280 (2014) 378–388

Contents lists available at ScienceDirect

Toxicology and Applied Pharmacology

journal homepage: www.elsevier.com/locate/ytaap

Development of a pluripotent stem cell derived neuronal model to identify chemically induced pathway perturbations in relation to neurotoxicity: Effects of CREB pathway inhibition

Francesca Pistollato [a], Jochem Louisse [a], Bibiana Scelfo [a], Milena Mennecozzi [a], Benedetta Accordi [b], Giuseppe Basso [b], John Antonydas Gaspar [c], Dimitra Zagoura [a], Manuela Barilari [a], Taina Palosaari [a], Agapios Sachinidis [c], Susanne Bremer-Hoffmann [a,*]

[a] Institute for Health and Consumer Protection (IHCP), JRC, Ispra, Italy
[b] Oncohematology Laboratory, Department of Woman and Child Health, University of Padova, Padova, Italy
[c] Center of Physiology and Pathophysiology, Institute of Neurophysiology, University of Cologne, Cologne, Germany

ARTICLE INFO

Article history:
Received 10 January 2014
Revised 1 July 2014
Accepted 11 August 2014
Available online 19 August 2014

Keywords:
Induced pluripotent stem cells
Embryonic stem cells
Neuronal derivatives
CREB pathway
KG-501

ABSTRACT

According to the advocated paradigm shift in toxicology, acquisition of knowledge on the mechanisms underlying the toxicity of chemicals, such as perturbations of biological pathways, is of primary interest. Pluripotent stem cells (PSCs), such as human embryonic stem cells (hESCs) and human induced pluripotent stem cells (hiPSCs), offer a unique opportunity to derive physiologically relevant human cell types to measure molecular and cellular effects of such pathway modulations. Here we compared the neuronal differentiation propensity of hESCs and hiPSCs with the aim to develop novel hiPSC-based tools for measuring pathway perturbation in relation to molecular and cellular effects in vitro. Among other fundamental pathways, also, the cAMP responsive element binding protein (CREB) pathway was activated in our neuronal models and gave us the opportunity to study time-dependent effects elicited by chemical perturbations of the CREB pathway in relation to cellular effects. We show that the inhibition of the CREB pathway, using 2-naphthol-AS-E-phosphate (KG-501), induced an inhibition of neurite outgrowth and synaptogenesis, as well as a decrease of $MAP2^+$ neuronal cells. These data indicate that a CREB pathway inhibition can be related to molecular and cellular effects that may be relevant for neurotoxicity testing, and, thus, qualify the use of our hiPSC-derived neuronal model for studying chemical-induced neurotoxicity resulting from pathway perturbations.

Introduction

In the vision and strategy document "Toxicity Testing in the 21st Century" of the US National Research Council (NRC), a paradigm shift in regulatory toxicity testing is envisioned from the current testing approach, relying on phenotypic changes in animals, to an approach focusing on understanding how chemical-induced perturbations of biological pathways can lead to toxic effects in humans ((NRC), 2007). The vision focuses on the identification of toxicity pathways, which are "normal cellular response pathways that are expected to result in adverse health effects when sufficiently perturbed" ((NRC), 2007). This means that toxicity pathways represent perturbations of biological pathways that cannot be recovered by adaptive stress responses, which will lead to cell injury and as a result to morbidity and mortality in vivo.

In the US-EPA screening project ToxCast, high-throughput screenings have been performed, in which chemicals have been assessed for the perturbation of key biological pathways (Dix et al., 2007; Judson et al., 2010). Some of the ToxCast data have already been analyzed to assess correlations between pathway perturbations and cellular/tissue injury, particularly in relation to developmental toxicity, impairment of vascular development and endocrine disruption (Chandler et al., 2011; Kleinstreuer et al., 2011; Sipes et al., 2011; Rotroff et al., 2013). In addition, the possible correlation between pathway perturbations and activation of adaptive stress responses should be taken into account in order to test whether a certain biological pathway can qualify as a toxicity pathway.

In the present study we aim to relate the perturbation of a biological pathway (the cAMP responsive element binding protein (CREB) pathway) to cellular effects in relevant human target cells (human induced pluripotent stem cell (PSC)-derived neuronal cultures).

PSCs are currently seen as a promising cell source for toxicological applications, as their derivatives exhibit normal, non-pathologic

* Corresponding author at: Via E. Fermi 2749, I-21027 Ispra (VA), Italy. Fax: +39 0332 785388.
E-mail address: susanne.bremer@jrc.ec.europa.eu (S. Bremer-Hoffmann).

http://dx.doi.org/10.1016/j.taap.2014.08.007

properties, which can be absent in models based on cancer cells. The two major types of PSC cultures that are most promising are human embryonic stem cells (hESCs) and human induced pluripotent stem cells (hiPSCs). Currently, hESCs as well as hiPSCs are widely used in the area of basic research and regenerative medicine (Drews et al., 2012; Ho et al., 2012). This expertise can now be harnessed for their application in in vitro toxicology. However, test methods for regulatory safety assessment based on hESCs would unlikely be accepted worldwide, due to diverse national legislative policies regulating the use of embryo-derived cell lines. An alternative to hESC-based assays might be the use of hiPSC-based assays for regulatory toxicity testing (Kumar et al., 2012). HiPSCs are commonly derived from fetal or adult somatic cells but still share similar characteristics with hESCs (Krueger et al., 2010; Pistollato et al., 2012) and hold a great potential for in vitro methods, both for identifying therapeutic targets as well as for safety assessment. Nevertheless, recent publications demonstrated the existence of some substantial epigenetic differences between hESCs and hiPSCs, with hiPSCs showing significant reprogramming variability, including somatic memory and aberrant reprogramming of DNA methylation, compared to hESCs (Daniels et al., 2010; Ghosh et al., 2010; Lister et al., 2011). Therefore, it is of interest to characterize and compare cellular derivatives of both PSC models in order to determine the suitability of PSC-derivatives for toxicological applications. Moreover, in light of the novel toxicity paradigm, these stem cell derivatives can be used to detect perturbations of pathways that may underlie the molecular and cellular events leading to cell injury. Here we differentiate hiPSCs (IMR90-hiPSCs) into post-mitotic neurons, comparing their differentiation efficiency to hESCs (H9), with the goal to correlate chemical-induced perturbations of the neuronal-related CREB pathway to molecular and cellular events that may play a role in neuronal cell injury.

The CREB pathway is crucial in the development of the central nervous system (CNS), including neuronal survival, neurite outgrowth, precursor proliferation and neuronal differentiation (Lonze and Ginty, 2002). It plays an important role in learning and memory formation, the entrainment of the circadian clock, as well as in addiction (Lonze and Ginty, 2002). A wide range of stimuli can activate CREB signaling in neurons, like hormones, neurotransmitters, growth factors and Ca^{2+}, but also stress (Shaywitz and Greenberg, 1999; Lonze and Ginty, 2002). CREB has been found altered in several neuronal diseases, like Huntington disease, the Coffin–Lowry syndrome, the Rubinstein–Taybi Syndrome and Alzheimer's disease (Saura and Valero, 2011). The relevance of the CREB pathway for the nervous system has also been demonstrated by toxicity studies that have related the perturbation of the CREB signaling pathway to neurotoxicity (Schuh et al., 2002; Chalovich et al., 2006; Damodaran et al., 2009; Zuo et al., 2009; Liu et al., 2010; Xu et al., 2011; Brunelli et al., 2012). Therefore, the CREB pathway is an interesting pathway to be explored as a toxicity pathway in relation to neurotoxicant exposure.

In order test effects of CREB pathway perturbations we used the specific CREB signaling inhibitor 2-naphthol-AS-E-phosphate (KG-501), administered in a time course fashion in our hiPSC-derived neuronal cultures. KG-501 caused an inhibition of neurite outgrowth and synaptogenesis and a decrease of $MAP2^{+}$ neuronal cells. Our data indicate that our hiPSC-derived neuronal cultures might be useful tools to study chemical effects on neuronal cells, providing a valuable alternative to the use of other in vitro cell models, such as cancer cell lines or animal cells.

Materials and methods

PSC lines and culture conditions. For this study, the H9 hESC cell line (obtained from WiCell, MTA number: 10-W0409) and the IMR90 hiPSC line (provided by I-Stem, Evry, France) have been used. The H9 line was derived from a supernumerary IVF embryo and the karyotype is 46,XX, indicative of a normal diploid female (https://www.wicell.org/index.php?option=com_content&task=view&id=206&Itemid=0); the IMR90 line was established on 07/07/1975 using explants of minced lung tissue obtained from a clinically normal 16 week old fetus. The karyotype is 46,XX, indicative of a normal diploid female (http://ccr.coriell.org/Sections/Search/Sample_Detail.aspx?Ref=I90-52&PgId=166). IMR90 cells had been reprogrammed in the laboratories of I-Stem towards pluripotency by retroviral transduction of Oct4 and Sox2, using the pMIG vectors (Addgene).

hESC and the hiPSC lines were grown on mitomycin-inactivated human feeder fibroblasts (hDFn, Gibco, Cascade Biologics), which have been plated on 0.1% gelatin (Sigma Aldrich) and diluted in 1× PBS (Gibco, Life Technologies). Cells were grown in 5% ± 1% CO_2/air in humidified incubators (37 °C ± 1 °C), and medium was changed every day with the addition of basic FGF (bFGF, Immunological Sciences) at the concentration of 8 ng/ml for hESCs and 10 ng/ml for hiPSCs (Supplementary Tables 1 and 2). PSC colonies were passaged by micro-dissection using a 30G needle and p100 μl tip and regrowth from small colony fragments on feeder cell layers. Normally, about 100 fragments were replated, with a plating efficiency of about 80%. To assess stem cell pluripotency, we used the common approach based on "spontaneous" embryoid body (EB) formation, which can form the three germ layers (Shamblott et al., 2001), followed by qPCR analyses of germ layer specific genes. Regular checking for potential mycoplasma contamination has been performed twice per month and before preparing frozen cell stocks by doing qPCR on an ABI PRISM® 7000 Sequence Detection System (Applied Biosystems) with a specific mycoplasma detection kit (Minerva Biolabs) on both cell supernatants and cell samples.

Differentiation protocol for post-mitotic neurons and time course treatment with 2-naphthol-AS-E-phosphate (KG-501). H9 and IMR90 cells were differentiated into post-mitotic neurons, as previously described (Stummann et al., 2009), with some modifications. Briefly, EBs were generated by detaching undifferentiated colonies by manual cutting of colonies into 200 μm × 200 μm fragments. Floating EBs were cultured for 1 day in the presence of complete hESC or hiPSC medium (Supplementary Tables 1 and 2) without bFGF. Then, on day 2, EBs were plated on laminin coated dishes (1 mg/ml stock, Sigma L2020, used at final concentration of 10 μg/ml in sterile mq water) in the presence of neural induction medium (NI, Supplementary Table 3) and maintained in culture for 1 week to promote early neural differentiation, performing a total medium change three times a week. Neuroepithelial aggregates, called rosettes, became visible, already after 48h and on day 8 were cut in fragments using a 30G needle and p100 μl tip, using a phase contrast microscope under sterile conditions. Fragments were partially dissociated using a p1000 tip and 1ml of PBS 1x and were replated on laminin coated dishes in the presence of neuronal differentiation medium (ND, Supplementary Table 4). Cells were cultured for at least 3 additional weeks to promote full maturation and differentiation performing a total medium change twice a week. At day 28 of differentiation (day 0 of toxicity test), IMR90-derived neuronal cells were exposed to 2-naphthol-AS-E-phosphate (KG-501, Sigma-Aldrich) up to 14 days, refreshing medium together with KG-501 treatment every 3–4 days and using DMSO as solvent control. Samples were collected for analyses at 3 h, 1 day, 3 days, 7 days and 14 days (Supplementary Fig. 5D). To evaluate delayed cytotoxicity, IMR90-neurons were treated for 3 h, 1 day, 3 days or 7 days, then KG-501 was withdrawn and medium was refreshed for additional 14 days, as indicated in Supplementary Fig. 5E.

Quantitative real-time PCR (qPCR) analyses. Analysis of gene expression by qPCR has been performed on undifferentiated cells, embryoid bodies, as well as neuroectodermal aggregates as well as in untreated and KG-501-treated differentiated cells. Cells were resuspended in 100 μl of cold RNA lysis buffer provided within the RNAqueous®-

Micro Kit (Life Technologies). RNA was isolated according to manufacturer's instructions and 0.5 μg of total RNA was reverse-transcribed using High Capacity cDNA Reverse Transcription Kits (as directed, Applied Biosystems). qPCR reactions were run in duplicate using TaqMan® Gene Expression Master Mix (Applied Biosystems) and several TaqMan Gene Expression Assays (Supplementary Table 5). Fluorescent emission was recorded in real-time (Sequence Detection System 7000HT, Applied Biosystems). PCR amplification conditions consisted of 40 cycles with primers annealing at 60 °C. Relative RNA quantities were normalized to GAPDH and β-actin as reference genes and undifferentiated H9 or IMR90 cells (at day 0), or untreated differentiated H9 or IMR90 cells were used as calibrating conditions (ΔΔCt Method). Additionally, TaqMan Human Stem Cell Pluripotency Array (Applied Biosystem, as directed) was used to compare undifferentiated H9 vs undifferentiated IMR90.

Immunocytochemistry and neurite outgrowth analyses by high content imaging (HCI). Analyses of pluripotency and neuronal-related markers were performed by using the Thermo Scientific Cellomics ArrayScan vTi for HCI. Briefly, undifferentiated (about 20 colony fragments/well in 96 well plates) and differentiated cells (about 6000 cells/well in 96 well plates) were fixed in cold 4% formaldehyde for 15 min, rinsed with PBS and stored at 4 °C prior to analysis. Staining for a wide range of primary antibodies was performed (Supplementary Table 6). After incubation, cells were washed and incubated with species-specific secondary antibodies conjugated to Alexa dyes (Invitrogen). Cell nuclei were counterstained with DAPI dye (0.3 μM, Sigma-Aldrich) to measure total live (i.e. non-pyknotic nuclei) cell numbers. Cells incubated with appropriate isotypic control antibodies were analyzed to ensure labeling specificity. Quality of staining was visualized by epifluorescence (Canon). Images were compiled for figures using CorelDRAW Graphics X5 (Corel). Quantification of mean fluorescence intensity and the relative percentages of cell types were calculated using a specific ArrayScan algorithm (Cytotoxicity V.4 BioApplication), which applies a specific nuclear mask around the DAPI staining, discarding invalid nuclei (i.e. pyknotic bright nuclei and/or clumps of cells) and, on the valid nuclei, a cell body shape mask designed according to the antibody/antigen staining (O'Brien et al., 2006). Secondary antibody incubation alone was used to determine the intensity level of fluorescent background to be subtracted. Neurite outgrowth was calculated on β-III-tubulin^{+} cells using a specific Thermo Scientific Cellomics ArrayScan vTi algorithm (Neurite Outgrowth V.4 BioApplication) that enables automated plate handling, focusing, cell image acquisition, analysis and neurite outgrowth quantification. As already reported (Radio, 2012), the Neurite Outgrowth algorithm identifies cell nuclei stained with DAPI (thick blue mask) and neuronal bodies stained with β-III-tubulin (thick orange mask) (Supplementary Fig. 2E). The neurites are then identified by a red mask and the branch points by a yellow mask. On the acquired images, the mathematical algorithm automatically measures the number of neurites per neuron, the length of the neurites (expressed in μm) and the number of branch points per neurite, which is indicative of neurite complexity level. For further information on this standardized method the following document can be consulted: http://www.thermoscientific.jp/cellomics/docs/LC01572000_NP_Application_note_Bova.pdf.

Reverse phase protein array (RPPA) assays and analysis. Reverse phase protein array analysis was performed as previously described (Accordi et al., 2010). In brief, protein lysates were printed in 4-point dilution curves in duplicate on nitrocellulose-coated slides (FAST slides; Whatman Schleicher & Schuell) with the 2470 Arrayer (Aushon BioSystems). Slides were stained for total protein content (Fast Green FCF; Sigma-Aldrich), and with 50 validated primary antibodies (Supplementary Table 7) using the Catalyzed Signal Amplification System kit (DAKO). The TIF images of antibody- and Fast Green FCF-stained slides were analyzed using the Microvigene software (VigeneTech Inc) to extract numeric intensity values from the array images.

Assessment of cell viability with Alamar Blue assay. To get a first indication on the cytotoxic effects of KG-501, neuronal cells were exposed for 3 h, 1 day, 2 days, 7 days or 14 days to KG-501 at concentrations ranging from 0.1 to 75 μM, after which cell viability was assessed using the Alamar Blue (resazurin) assay. To this end, the medium containing KG-501 was removed and cells were incubated with 10 μM resazurin (diluted in ND medium) keeping the plates for 2 h in the incubator (37 °C, 5% CO_2). Subsequently, the fluorescence of resorufin was measured at 530–560 nm/590 nm (excitation/emission) in a multiwell fluorimetric reader (Tecan). The results were normalized to the mean of untreated cells (control).

Gene expression profiling of undifferentiated and differentiated PSC samples. Total RNA was extracted using trizol/chloroform and purified with RNeasy mini columns as recommended by the manufacturer's instructions (Qiagen, Hilden, Germany). All reagents and instrumentation pertaining to oligonucleotide microarrays were procured from Affymetrix (Affymetrix, Santa Clara, CA, USA, http://www.affymetrix.com). Total RNA (100 ng) was used for amplification and in-vitro transcription using the Genechip 3′ IVT Express Kit following the manufacturer's instructions (Affymetrix). The amplified RNA was purified with magnetic beads and 15 μg of Biotin-RNA was fragmented with a fragmentation reagent. 12.5 μg of fragmented RNA was hybridized to Affymetrix Human Genome U133 plus 2.0 arrays along with hybridization cocktail solution and then placed in Genechip Hybridization Oven-645 (Affymetrix) rotating at 60 rpm at 45 °C for 16 h. After incubation arrays were washed on Genechip Fluidics Station-450 (Affymetrix) and stained with Affymetrix HWS kit following the manufacturer's protocols. The chips were scanned with Affymetrix Gene-Chip Scanner-3000-7G and the quality control matrices were confirmed with Affymetrix GCOS software following the manufacturer's guidelines.

Determination of significantly altered gene profiling between undifferentiated and differentiated samples. Robust Multi-array Analysis algorithm (RMA) did background correction, summarization and normalization. Quantile normalization method (Bolstad et al., 2003) was employed to normalize the raw dataset at probe feature level executable with R (Affy)-package (Gautier et al., 2004). Linear model implementing R-LIMMA packages (Linear Models for microarray data) (Smyth, 2004) describes the significantly altered gene profile. For statistical filtration of differentially regulated genes, cut-off values of 5% error rate ($p < 0.05$) estimated by moderated *t*-statistics with Benjamini and Hochberg Multiple Testing Correction along with the fold change threshold value ≥ (plus minus) 2.0 were used. K-Mean cluster analysis was performed after transcript-wise normalization of signal values to a mean of 0 and standard deviation of 1 using Euclidian distance measurement and $k = 7$, using Cluster 3.0 tool from Eisen lab (Eisen et al., 1998).

Statistical analysis. Graphs were prepared and statistical analyses were performed using Graph Pad Prism version 5. All values are presented as mean ± standard error of the mean (SEM). Statistical significance was assessed by one-way ANOVA with Dunnett's multiple comparisons test or by 2-tailed unpaired or paired *t*-test according to the type of analysis. For all graphs, an asterisk (*) over a bar or over a bracket indicates a significant difference (i.e. $p < 0.05$) with the control group (i.e. either undifferentiated or untreated cells), unless otherwise specified in the figure legend.

Results

Characterization of undifferentiated H9-hESCs and IMR90-hiPSCs and analysis of pluripotency

A high level of standardization of undifferentiated cell cultures as well as of the differentiation process is required in order to ensure the establishment of robust test systems using PSC-derived cells (Pistollato et al., 2012). We first analyzed the gene expression profile comparing undifferentiated IMR90-hiPSCs with undifferentiated H9-hESCs in order to evaluate the similarity of the two PSC types. Quantitative real time PCR (qPCR) analyses of undifferentiation/pluripotency related genes, by using the Taqman human pluripotency array, showed quite similar profiles comparing undifferentiated H9 vs IMR90, except for the slightly higher expression of GBX2, LIFR, NODAL and Xist genes in IMR90 than in H9 (Supplementary Fig. 1A) (not significantly different). In particular, Xist (X-inactive specific transcript) is a major effector of the X inactivation process and its expression is variable in female undifferentiated hESCs (Shen et al., 2008; Silva et al., 2008; Lengner et al., 2010) and hiPSCs (Tchieu et al., 2010; Bruck and Benvenisty, 2011), which may reflect some variability in the epigenetic state and developmental potential of these cell types. Moreover, undifferentiated H9 and IMR90 cells were stained by the pluripotency related markers Oct4, SSEA3 and Tra1-60 (Supplementary Fig. 1B), while percentages of nestin$^+$ and β-III-tubulin$^+$ cells were low (Supplementary Fig. 1B). In addition, stem cell pluripotency was analyzed by "spontaneous" embryoid body (EB) formation, which induces the formation of the three germ layers (Shamblott et al., 2001). Analyses of germ layer specific genes indicated that both H9 and IMR90 cells underwent a similar increase of endodermal (AFP, KRT18), ectodermal (Nestin, Sox1 and Pax6) and mesodermal (NPPA and Brachyury-T) related gene expression (Supplementary Figs. 1C, D). Comparing the two cell lines, a higher Pax6 and AFP expression was observed in IMR90-derived EBs than in H9-derived EBs, as compared to their respective undifferentiated controls (dotted lines, Supplementary Figs. 1C, D), which might reflect some differences in pluripotency and/or some diverging differentiation tendencies between the two cell models.

Characterization of H9-hESC- and IMR90-hiPSC-derived post-mitotic neurons and glia

A thorough characterization of PSC-derivatives is needed when aiming to use PSC-derived cultures to assess the effects of pathway perturbations in relation to neuronal cell injury.

We differentiated H9-hESCs and IMR90-hiPSCs into post-mitotic neurons, according to our previously described protocol (Stummann et al., 2009) (Figs. 1A–C and 2A–F). We characterized the differentiated cultures by performing the following assays: (i) analyses of neuronal and glia specific genes and proteins; (ii) analyses of neurite-related parameters; (iii) characterization of the neuronal subtypes; (iv) whole gene expression profiling followed by the analysis of signaling pathways; and (v) analysis of neuronal-related pathways at the protein level.

By applying our neuronal differentiation protocol (Fig. 1A), rosette-like structures started to become visible 5–8 days after EB plating in the presence of neural induction (NI) medium (Figs. 1B, C (rosettes at day 7)). Importantly, the majority of the cells were nestin$^+$ and β-III-tubulin$^+$ cells within these structures, indicative of neuronal precursors and immature neurons, and were localized mainly at the periphery of the rosettes (colored insets, Figs. 1B, C). Immunostaining and high content imaging (HCI) on the differentiated cultures (28 days of differentiation) showed a decrease of pluripotency related markers in differentiated vs undifferentiated cells, together with a decrease in the number of Ki67$^+$ cells, a well described cell cycle marker (significant only in differentiated IMR90 neuronal cultures) (Supplementary Fig. 2A). By contrast, an increase of neuronal cells, such as β-III-tubulin$^+$, MAP2$^+$ and NF200$^+$ cells, occurred upon differentiation in the two cell models (Figs. 2A–C and F, Supplementary Fig. 2B). Moreover, we detected a modest proportion of neural stem nestin$^+$ cells

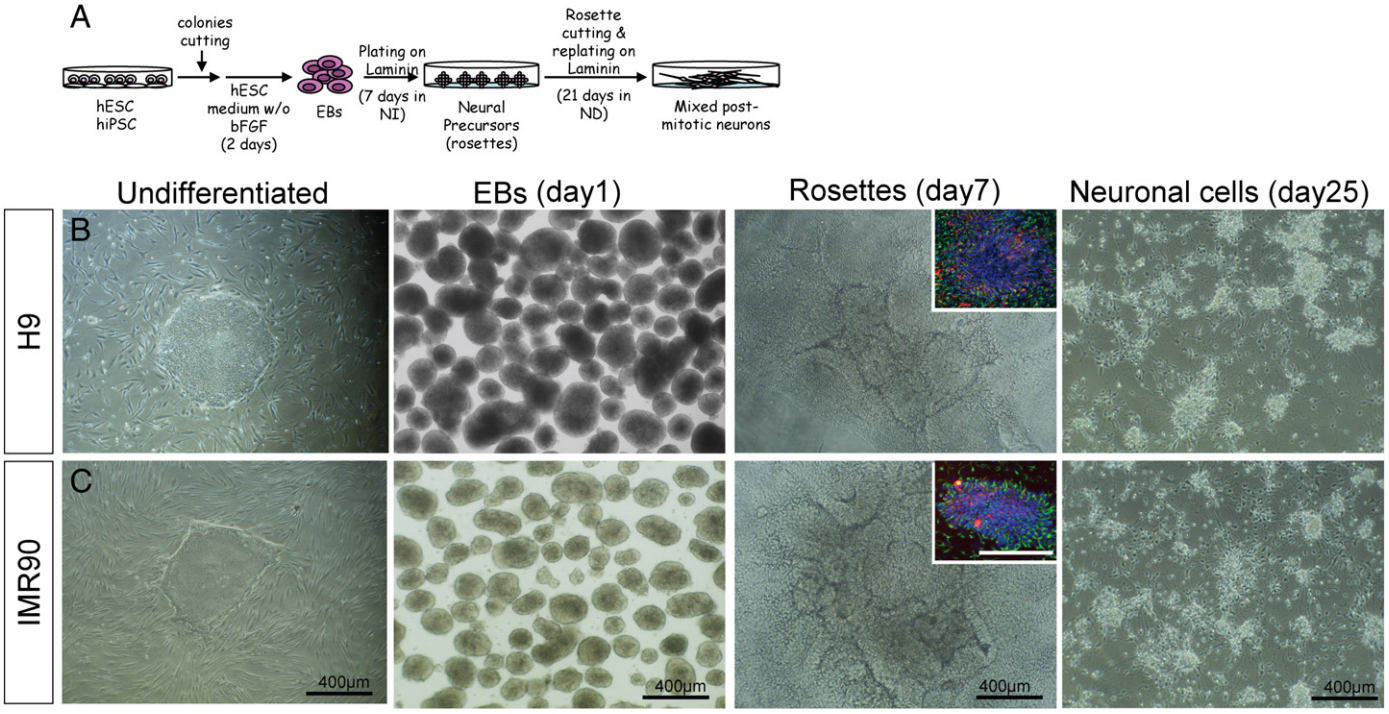

Fig. 1. Neuronal differentiation of PSCs. (A) Representative scheme summarizing the described neuronal differentiation protocol. (B, C) (From the left) Representative phase-bright images of undifferentiated colonies (H9 p35 and IMR90 p40), of EBs at day 1, of rosettes at day 7, with 20× magnification insets showing nestin$^+$ (green) and β-III-tubulin$^+$ cells (red) (bar = 200 µm) and of neuronal cells at day 25.

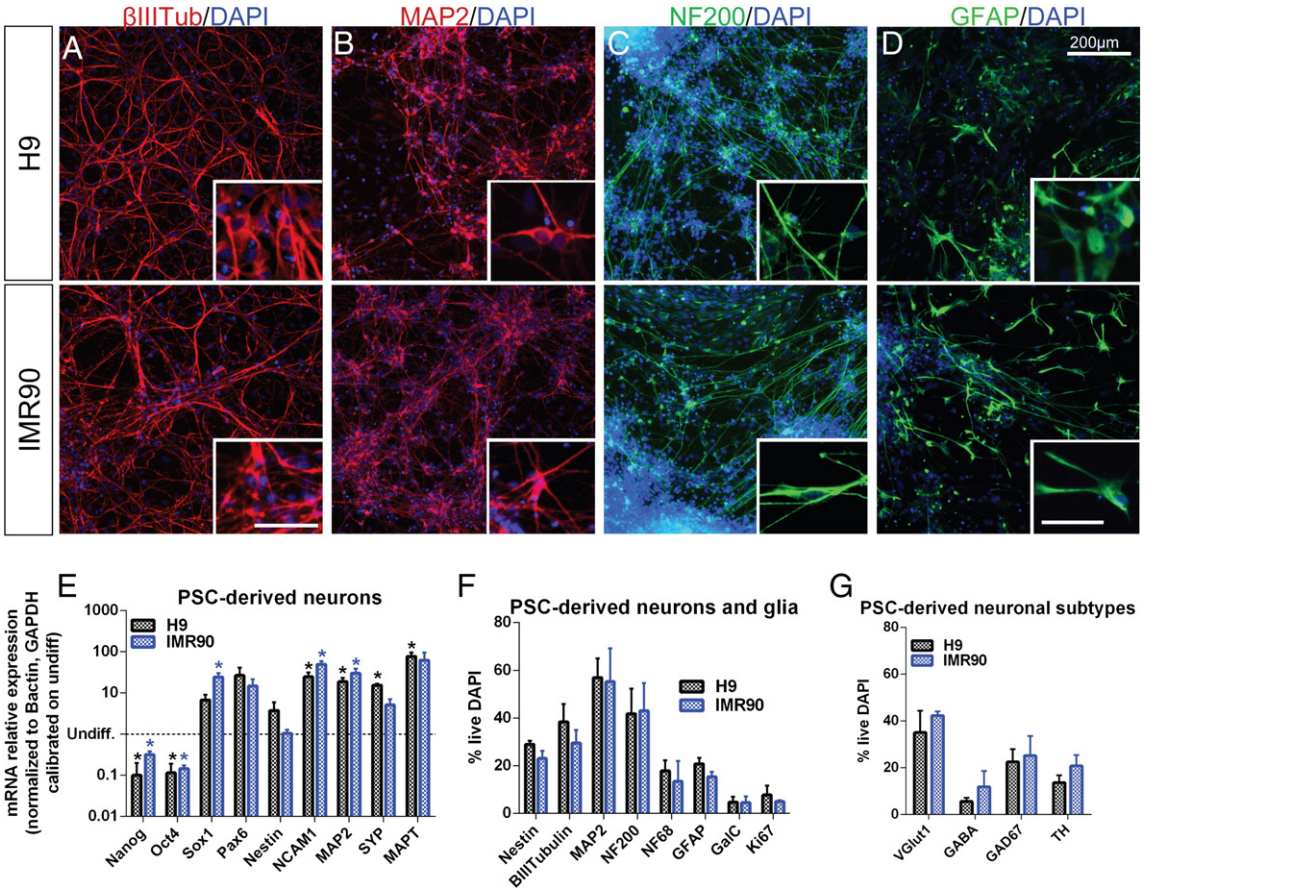

Fig. 2. Both hESC-H9 and hiPSC-IMR90 cells after 28 days differentiate toward neurons and glia. (A–D) Representative immunocytochemical images of β-III-tubulin (Tuj1, red), MAP2 (red), NF200 (green) and GFAP (green) (insets with bar = 100 μm) (H9 p37, IMR90 p42). (E) Bar graph reporting qPCR analyses of indicated genes, all normalized to β-actin and GAPDH and then calibrated to undifferentiated H9 or IMR90 cells (for both, dotted line) (ΔΔCt method). Mean ± SEM of 6 independent analyses for IMR90 and of 4 independent analyses for H9. (F) Bar graph reporting % of indicated cell markers on total live DAPI + cells, mean ± SEM of 5 independent analyses for both cell lines. (G) Bar graph reporting percentages of different neuronal cell sub-populations on total live DAPI$^+$ cells (mean of 3 independent analyses ± SEM for both cell lines).

(20–25% of total DAPI$^+$ cells, Fig. 2F) in the differentiated cultures. Additionally, we found that H9 and IMR90 differentiated cultures were also characterized by the presence of about 15–20% of GFAP$^+$ cells, indicative of astroglia (Fig. 2D, F) and 4% of GalC$^+$ cells, indicative of mature oligodendrocytes (Fig. 2F). Interestingly, by differentiating the two cell culture types for longer times (i.e. 5–8 weeks) we could not detect significant differences compared to cells differentiated for 4 weeks (Supplementary Figs. 2C, D).

qPCR analysis on H9 and IMR90 cells undergoing differentiation showed a similar downregulation of the pluripotency-related genes Oct4 (POU5F1) and Nanog, starting from day 4 of differentiation (Fig. 2E and Supplementary Figs. 3A, B). Conversely, the neuroectodermal related genes Pax6 and Sox1 were upregulated three times more than the undifferentiated cells up to day 12 of differentiation, reaching a plateau later on during differentiation, while nestin expression did not change (Supplementary Figs. 3C, D). Furthermore, a marked increase in the expression levels of the neuronal related genes NCAM1 and MAP2 was observed in both H9 and IMR90-derived neuronal cells as compared to their undifferentiated counterparts (Fig. 2E and Supplementary Figs. 3E, F). Additionally, qPCR analyses of synaptophysin (SYP) and microtubule-associated protein tau (MAPT), the former expressed at the synaptic level, the latter in distal portions of axons, revealed an increase of expression upon differentiation (Fig. 2E).

By using a specific HCI algorithm to analyze the number, the length and the level of complexity of the neurites, based on β-III-tubulin staining (Supplementary Fig. 2E), we found that H9 and IMR90-derived neurons formed different types of neurites. IMR90-neurons were characterized by the presence of a higher number of neurites/neurons, but were shorter and structurally less complex (i.e. with less branch points), than the ones formed by H9-neurons (Supplementary Fig. 2F). This might reflect some differences between the two cellular models in the neuronal polarization capability (Yamamoto et al., 2012).

We sought to better characterize the neuronal subtypes present in our differentiated cell cultures. Our HCI data showed that both the differentiated cell models were characterized by a high percentage of the two major types of forebrain neurons, glutamatergic (VGlut1$^+$, ~35% for H9 and ~42% for IMR90) and GABAergic neurons (GABA$^+$, ~6% for H9 and ~11% for IMR90 and GAD67$^+$, ~22% for H9 and ~25% for IMR90) (Fig. 2G and Supplementary Figs. 4A, B). Importantly, also a proportion of dopaminergic neurons were present in both differentiated cell models (TH$^+$, ~13% for H9 and ~20% for IMR90) (Fig. 2G and Supplementary Figs. 4A, B). Cholinergic neurons (ChAT$^+$ cells) were not represented in both cell cultures. qPCR analyses mainly confirmed HCI data, indicating that especially dopaminergic, noradrenergic, glutamatergic and GABAergic-related genes were upregulated in both H9 and IMR90-derived neuronal cells compared to undifferentiated cells, together with motor neuron and cholinergic-related genes (Supplementary Fig. 4C). However, some genes (i.e. GABRA1 and LHX3) resulted differentially expressed comparing differentiated H9 vs differentiated IMR90 (Supplementary Fig. 4C), indicating a possible difference in transcriptional regulation of the neuronal differentiation process between the two cell types.

Furthermore, we performed a complete gene expression profiling using 3′ IVT gene expression analysis using Affymetrix. By comparing undifferentiated H9 and IMR90 against their differentiated counterparts, we retrieved 7 gene clusters (Supplementary Fig. 5A). Particularly, cluster 1 was representative of 1523 genes/probes that resulted upregulated upon neuronal differentiation in both the cellular models (Fig. 3A), cluster 3 comprised 1319 genes/probes that resulted mainly downregulated upon neuronal differentiation and cluster 4 grouped a relatively small number (141) of genes/probes that were generally upregulated in IMR90 cells, regardless their status (i.e. undifferentiated and/or differentiated) vs H9 cells (see annexed "Specific gene clusters 1-3-4" xls file). By performing a KEGG pathway analysis, using the DAVID Functional Annotation Bioinformatics Microarray Analysis software (http://david.abcc.ncifcrf.gov/), we found that a high number of the upregulated genes/probes included in cluster 1 (Fig. 3A) were related to focal adhesion, MAPK signaling, endocytosis, Wnt signaling, neurotrophin and axon guidance (Fig. 3B); cluster 3 comprised genes involved in signaling pathways, such as purine metabolism, cell cycle, pyrimidine metabolism, RNA degradation, metabolism of several amino acids and tight junction regulation (Supplementary Fig. 5B); and cluster 4 grouped genes, unrelated to an undifferentiated or a neuronal phenotype, but related to focal adhesion, regulation of actin cytoskeleton, gonadotropin-releasing hormone (GnRH) signaling and leukocyte transendothelial migration (Supplementary Fig. 5C).

Additionally, we sought to evaluate specifically which neuronal related signaling pathways were activated at the protein level in the two cellular models upon neuronal differentiation. Analyses by reverse phase phosphoproteomic array (RPPA) confirmed the gene expression data, showing that a specific neuronal signature was similarly upregulated in both differentiated H9 and IMR90 cells (Fig. 3C). In particular, among the 50 analyzed proteins (Supplementary Table 7), identified by using antibodies specific for phosphorylated and total protein isoforms, we found Erk/CREB, Notch1, Akt/PDK1/mTOR, Shh, Wnt, SAPK/JNK and Smad-1,5,8 pathway related proteins upregulated/activated upon differentiation (Fig. 3C).

Effects of exogenous CREB signaling inhibition by 2-naphthol-AS-E-phosphate (KG-501)

Because of the relevance of the CREB pathway in relation to neuronal diseases (Saura and Valero, 2011) and neurotoxicity (Schuh et al., 2002; Chalovich et al., 2006; Damodaran et al., 2009; Zuo et al., 2009; Liu et al.,

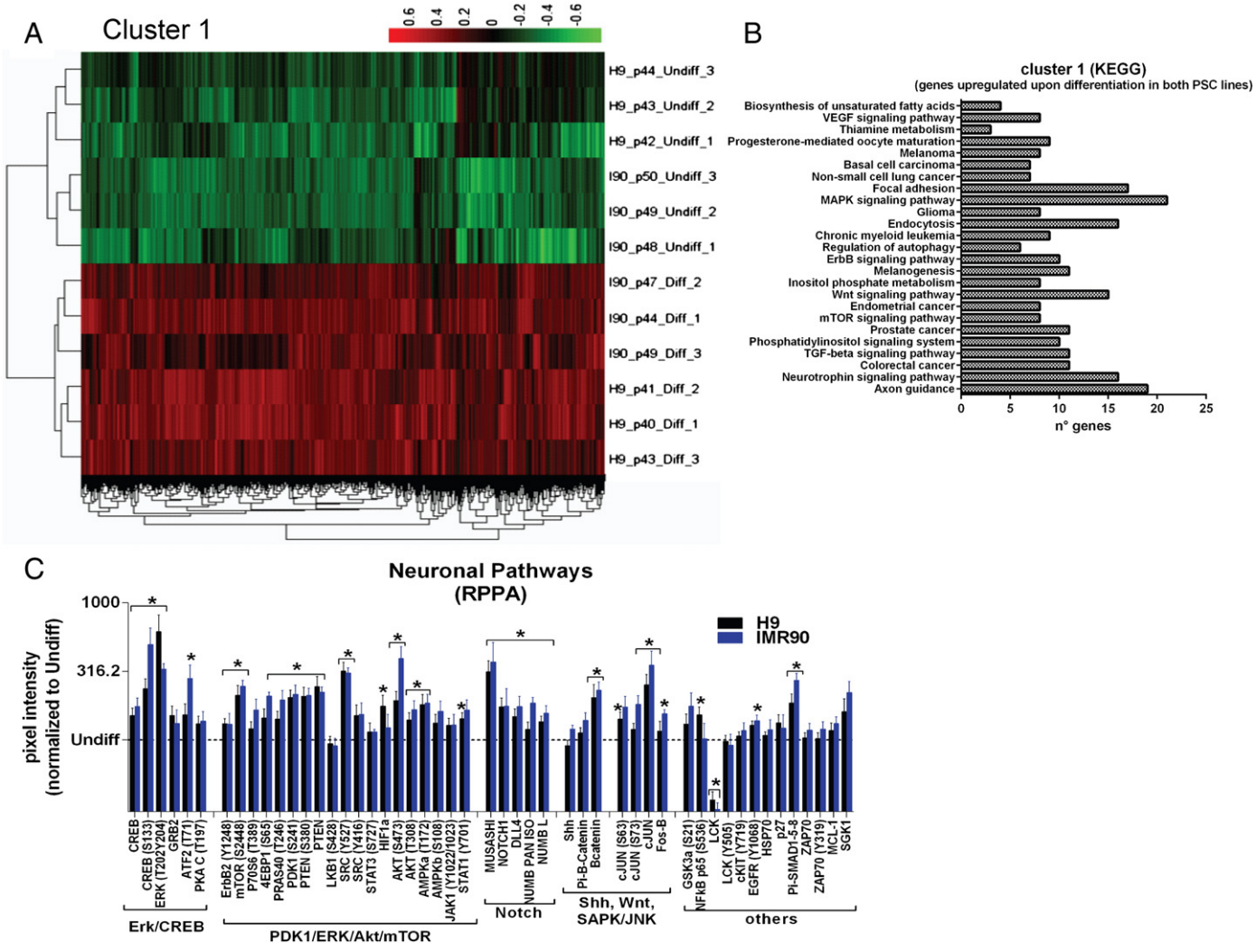

Fig. 3. H9 and IMR90-derived neuronal cultures undergo upregulation/activation of neuronal related genes and proteins. (A) Heatmap resulting from microarray analysis reporting genes/probes comprised into cluster 1 (genes upregulated upon differentiation in both cell cultures). Analysis is representative of three independent runs for all the conditions (undifferentiated and differentiated samples). (B) Bar graph reporting KEGG pathway analysis on cluster 1. (C) Bar graph reporting absolute protein quantifications normalized to their respective undifferentiated samples (for both cell lines, dotted line) using the Microvigene software, following RPPA analyses, comparing differentiated H9 (black bars) and differentiated IMR90 (blue bars). Analyzed proteins have been clustered together as indicated: Erk/CREB pathway, Notch1 pathway, PDK1/Erk/Akt/mTOR pathway, Shh, Wnt, SAPK/JNK pathways and other neural related pathways (mean ± SEM of 4 independent analyses for both the cell models).

2010; Brunelli et al., 2012), we investigated the effects of a time-dependent inhibition of CREB signaling in our hiPSC-neuronal model. To this end, we exposed the hiPSC-derived neuronal cultures up to 14 days to the specific CREB inhibitor 2-naphthol-AS-E-phosphate (KG-501) (see treatment scheme in Supplementary Fig. 5D) and we assessed both CREB signaling pathway- (i) and specific neuronal-related endpoints (ii). KG-501 is known to disrupt the CREB:CBP complex and attenuates target gene induction in response to cAMP agonists (Best et al., 2004) (Fig. 4A).

To get a first indication on the cytotoxic effects of KG-501, neuronal cells were assessed for cell viability using the Alamar Blue (resazurin) assay performed after 3 h, 1 day, 2 days, 7 days and 14 days of KG-501 treatment, applying KG-501 concentrations ranging from 0.1 to 75 μM (Fig. 4B). These data show that KG-501 induced a decrease of cellular resorufin formation (as a surrogate for cell viability) in a time dependent manner. Particularly, we found that KG-501 at the concentration of 25 μM, which has been reported to almost completely block CREB downstream gene expression in a reporter gene cell system (Best et al., 2004), decreased cell survival in IMR90-derived cells after 7-day exposure, while no effect on cell viability was observed in the short term (i.e. after 3 h, 1 day and 2 days) (Fig. 4B).

We then assessed the time dependent effects of 25 μM KG-501 (Supplementary Fig. 5D) on some CREB signaling pathway-related endpoints. We first analyzed the effects of KG-501 on the relative amount and the localization of phosphorylated CREB protein (pCREB (S133), using HCI) as well as the relative expression of selected CREB downstream genes (using qPCR) (Figs. 4C, D). Our data indicate that KG-501 treatment did not evoke an early (i.e. 3 h) effect on pCREB-(S133) levels, which is in accordance with previous report on forskolin treated HEK293T cells (Best et al., 2004). However, upon 1 day and 3 days of KG-501 exposure, we found a higher percentage of pCREB-(S133)$^+$ cells, presenting staining both in the cytoplasm as well as in the nucleus (Fig. 4D). However, after 14 days of KG-501 treatment pCREB levels resulted comparable to control (Fig. 4C).

Gene expression analyses indicate that 25 μM KG-501 induces different effects on the expression of the selected CREB downstream genes (Fig. 4D). Particularly, BDNF-AS1 (brain derived neurotrophic factor) expression, which is critical for neuronal survival, morphogenesis and plasticity (Numakawa et al., 2010), already decreased on day-3 of KG-501 exposure, whereas no effects were found at earlier time points (i.e. 3 h and 1 day). Interestingly, the monoamine vesicular transporter related gene SLC18A1, which allows the transport of biogenic monoamines, such as serotonin, from the cytoplasm into the secretory vesicles (Essand et al., 2005), was the most sensitive to KG-501 treatment, as a decrease was already observed after 3 h (Fig. 4D). Moreover, the expression of NR4A2 (Nurr1), which is related to dopaminergic neuron physiology (Sacchetti et al., 2006), was transiently increased at 3 h and 1 day, whereas no effect was found at later time points (i.e. 3 days, 7 days and 14 days) (Fig. 4D). FOS expression, which is indirectly related to neuronal activity (Dragunow and Faull, 1989; VanElzakker et al., 2008) (Day et al., 2008), resulted upregulated starting from 1-day exposure (Fig. 4D), while no effect was observed on the expression of PPARGC1 (PGC1), a regulator of mitochondrial biogenesis and function (Wu et al., 1999) (Fig. 4D). When analyzing the same CREB-related endpoints on IMR90-derived neurons that have been treated with lower concentrations of KG-501 (i.e. 1.2 and 6 μM) for 3 h, 1 day, 3 days, 7 days or 14 days, no significant changes in CREB-related gene expression were observed (see 6 μM KG-501 treatment in Supplementary Fig. 6A).

In order to evaluate whether KG-501-induced inhibition of CREB signaling resulted in detectable neuronal cell injury in IMR90-derived neuronal cultures we assessed the effects of a 3-h, 1-day, 3-day, 7-day and

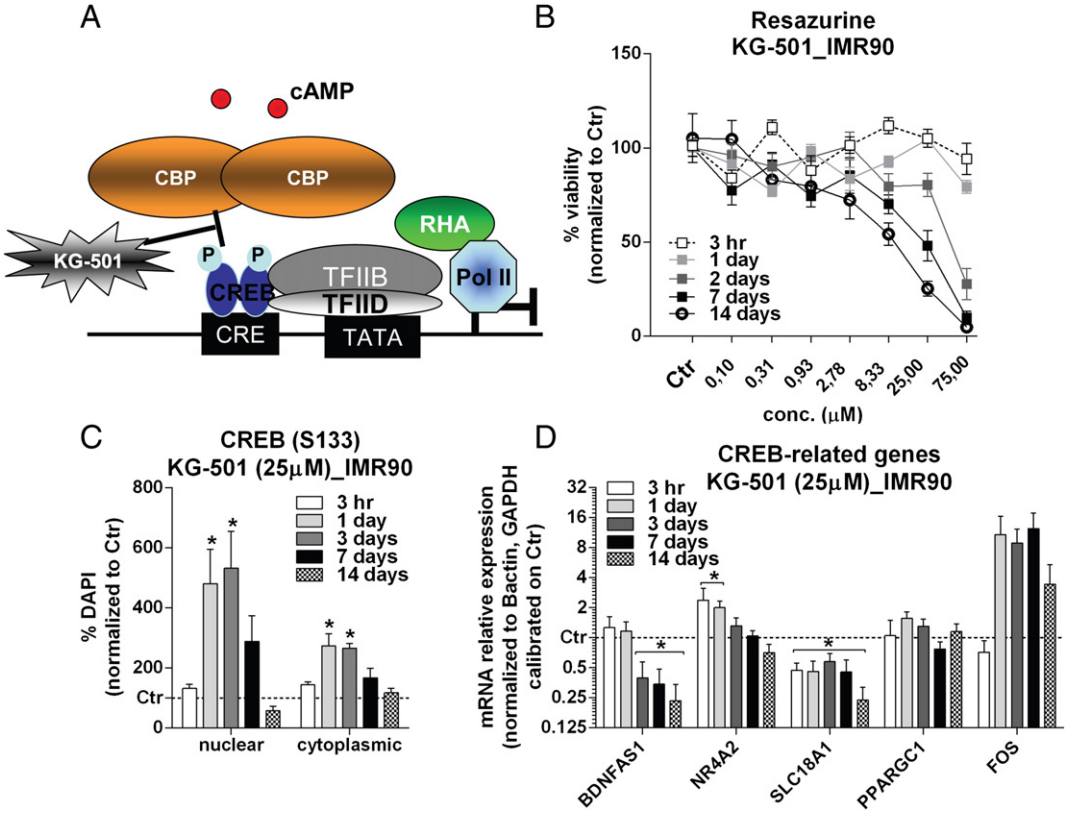

Fig. 4. Effects of KG-501 on CREB-related events in IMR90-derived neuronal cultures. (A) Cartoon summarizing KG-501's effect at the molecular level. (B) Concentration-dependent effect on neuronal survival upon a 3-h, 1-day, 2-day, 7-day and 14-day exposure, measured by the Alamar Blue assay. (C, D) Analysis on the effect of a time-dependent 25 μM KG-501 exposure on cytoplasmic and nuclear pCREB expression levels, analyzed by HCI (C), and mRNA expression levels of selected CREB related genes (D). Gene expression was normalized to β-actin and GAPDH and then calibrated to untreated cells (Ctr, dotted line, ΔΔCt method). For B, C and D, values were normalized to untreated cells (Ctr). For all the analyses, mean ± SEM of 3–4 analyses are shown.

14-day exposure to 25 μM KG-501 on the total number of cells (Fig. 5A), the fraction of β-III-tubulin$^+$, MAP2$^+$, NF200$^+$ and GFAP$^+$ cells (Figs. 5B and D, upper panels), neurite outgrowth, neurite length, the number of neurites per neuron and the number of branch points per neurite (Figs. 5C and D, lower panels), all measured by HCI, and the expression of synaptogenesis-related genes (Fig. 5E). In accordance to the viability test (Fig. 4B), we found a significant reduction of total live cell numbers starting from 7-day exposure to 25 μM KG-501 (Fig. 5A). Additionally, a remarked decrease of MAP2$^+$ neuronal cells was already observed after 3 days of KG-501 exposure (Figs. 5B and D, upper panels). The numbers of β-III-tubulin$^+$, NF200$^+$ and GFAP$^+$ cells did not show significant changes upon KG-501 exposure (Fig. 5B). Moreover, KG-501 induced a decrease in neurite length, number of neurites/neuron and number of branch points/neurite, which were already affected at early time points (i.e. 3 h and day 1) (Figs. 5C and D, lower panels). Moreover, a significant decrease of synaptophysin (SYP, expressed at the synaptic level) occurred on day-3 of KG-501 exposure, while a decrease of microtubule-associated protein tau (MAPT, expressed in distal portions of axons), which is indicative of synapses/synaptogenesis reduction, was visible after 7 days (Fig. 5E).

Assess whether the early effects (i.e. at 3 h, 1 day and 3 days) elicited by 25 μM KG-501 were possibly preceding delayed cytotoxicity, we performed "washout" experiments as depicted in Supplementary Fig. 5E. A single 3 h, 1 day or 3 day exposure to 25 μM KG-501, followed by KG-501 withdrawal and medium refreshment for 14 days (i.e. same "washout" period for all the time points), did not result in decrease of cell viability, as shown by quantitation of total live cell numbers (i.e. non-pyknotic nuclei, Supplementary Fig. 5F). When IMR90-neurons were exposed for 7 days to 25 μM KG-501, the cell number at day 21 (i.e. after the 14 day washout period) was similar to the one recorded at day 7 (Supplementary Fig. 5F, Fig. 5A), indicating no further delayed effects on cell viability at day 21. These data indicate that the observed early effects (i.e. the reduction of BDNF-AS1 and SLC18A1 gene expression, Fig. 4E, and the decrease of MAP2 + cells and neurites, Figs. 5B–D), should be attributed to a perturbation of CREB signaling induced by 25 μM KG-501 under non-cytotoxic conditions. Moreover, the 7 day exposure to 25 μM KG-501 (i.e. a prolonged perturbation of CREB signaling) seems to irreversibly impact neuronal cell viability.

Finally, 6 μM KG-501 treatment did not produce any significant change of selected neuronal endpoints at the same exposure times (Supplementary Figs. 6B–E).

In summary, the data on the effects of KG-501 in our hiPSC-derived neurons indicate that perturbation of the CREB signaling pathway early impacts neurite outgrowth and neuronal complexity, causes a decrease of MAP2$^+$ cells and of synaptogenesis-related gene expression in the medium term (i.e. after 3 days), and in the long term (i.e. after 7 days), a decrease of total cell number and cell survival occurs.

Discussion

In the present study we describe a robust and relatively rapid protocol for the differentiation of hiPSCs (IMR90-hiPSCs) into heterogeneous cultures of post-mitotic neurons and glia, comparing the differentiation potential of these cells to hESCs (H9), with the aim to investigate, in the hiPSC neuronal model, the time-dependent (adverse) cellular effects elicited by inhibition of the CREB signaling pathway using the specific CREB inhibitor KG-501. The obtained data may be useful in the understanding of how chemical-induced CREB inhibition relates to neuronal cell injury. Moreover, this model may be further applied to assess whether perturbation of the CREB pathway may be relevant to screen for neurotoxicants, and as such, qualify CREB pathway inhibition as a toxicity pathway.

In order to screen chemicals for the perturbation of pathways, signaling-reporter gene assays, as used in the TOXCAST program, may be useful tools. However, these assays do not give insight whether the possible observed pathway perturbations lead to cell injury. Therefore, in order to predict toxic cellular outcomes, it is important to assess the relation of pathway perturbation to toxic effects in specific cell types. Also, it may be relevant to predict whether the perturbation of a given pathway will result in (adverse) effects in cells of specific tissues/organs and, in this regard, heterogeneous cell derivatives, such as our hiPSC-derived neuronal cultures, rather than homogenous cell cultures, might better mimic possible toxicological responses in human tissues in vivo.

Currently, the use of PSC-derived, and particularly, of hiPSC-derived cells for regulatory toxicity testing has been taken into great consideration (Kumar et al., 2012), given the capability of hiPSCs to generate disparate toxicologically relevant cell types, avoiding the diverse national legislative policies regulating the use of hESC-derived models and the possible low scientific reliability related to the use of animal and cancer-derived cell lines. Defining reproducible differentiation protocols, yielding heterogeneous cultures of toxicologically relevant cell types, including progenitor/transit amplifying cells and terminally differentiated cells is needed to predict physiological in vivo cellular responses (Trosko and Chang, 2010). In this regard, the detection/permanence of a modest proportion of neural stem nestin$^+$ cells in our differentiated cell cultures (Fig. 2F) indicates that the models might be used to assess whether chemicals may particularly target the neural stem cell population in neuronal tissues, which is considered the cell fraction mostly affected by chemically induced mutations or viral infections (Canovas-Jorda et al., 2014), also according to the cancer stem cell theory (Sell, 2010). We show that both types of PSC models can be differentiated into heterogeneous cultures of GABAergic, glutamatergic and dopaminergic neurons, together with glial cells. Importantly, glial cells are fundamental for myelin formation, for the physiological functionality of neuronal networks and for neuronal homeostasis (Ghosh et al., 2011). Additionally, both PSC-derivatives are characterized by a similar neuronal signature, with some critical neuronal related signaling pathways upregulated and activated upon differentiation. The relatively small differences we observed between H9 and IMR90-derivatives, such as the diverse neurite profiling (Supplementary Fig. 2F), are not necessarily due to the fact of being natural ESCs or artificial iPSCs, respectively. Indeed, also hESC lines of different origins have been shown to vary in their differentiation propensity using the same differentiation protocol (Osafune et al., 2008).

Among the neuronal pathways that resulted upregulated/activated in both the differentiated cell models, the CREB pathway is of high relevance for several reasons. CREB plays a central role in the development and in the physiology of the CNS (Shaywitz and Greenberg, 1999; Lonze and Ginty, 2002) and has been reported to be affected by several toxicants, such as diisopropylphosphorofluoridate (Damodaran et al., 2009), chlorpyrifos (Schuh et al., 2002), 6-hydroxydopamine (Chalovich et al., 2006), non-dioxin-like polychlorinated biphenyls (Brunelli et al., 2012), perfluorooctane sulfonate (Liu et al., 2010), tributyltin and trimethyltin (Zuo et al., 2009). This indicates that the perturbation of the CREB pathway may play a role in chemical-induced neurotoxicity, and as such CREB might represent a relevant toxicity pathway for neurotoxicants.

To study the relevance of the CREB pathway as a possible neurotoxicity pathway we assessed the time-dependent molecular and cellular effects elicited by the specific CREB inhibitor KG-501 in our hiPSC-derived neuronal cultures. Upon KG-501 treatment, hiPSC-neurons activated pro-survival and/or stress-related responses, characterized by the immediate upregulation of NR4A2 and the downregulation of SLC18A1 gene expression, occurring within 3 h, together with an impairment of neurite length and neurite complexity. A transient activation of CREB and upregulation of FOS gene occurred within 1 day of KG-501 exposure (early effects). We also measured a progressive loss of neuronal functionality and survival, as shown by the time dependent downregulation of BDNF-AS1 and SYP expression and the decrease of the number of neurites and of MAP2$^+$ neuronal cells, occurring after

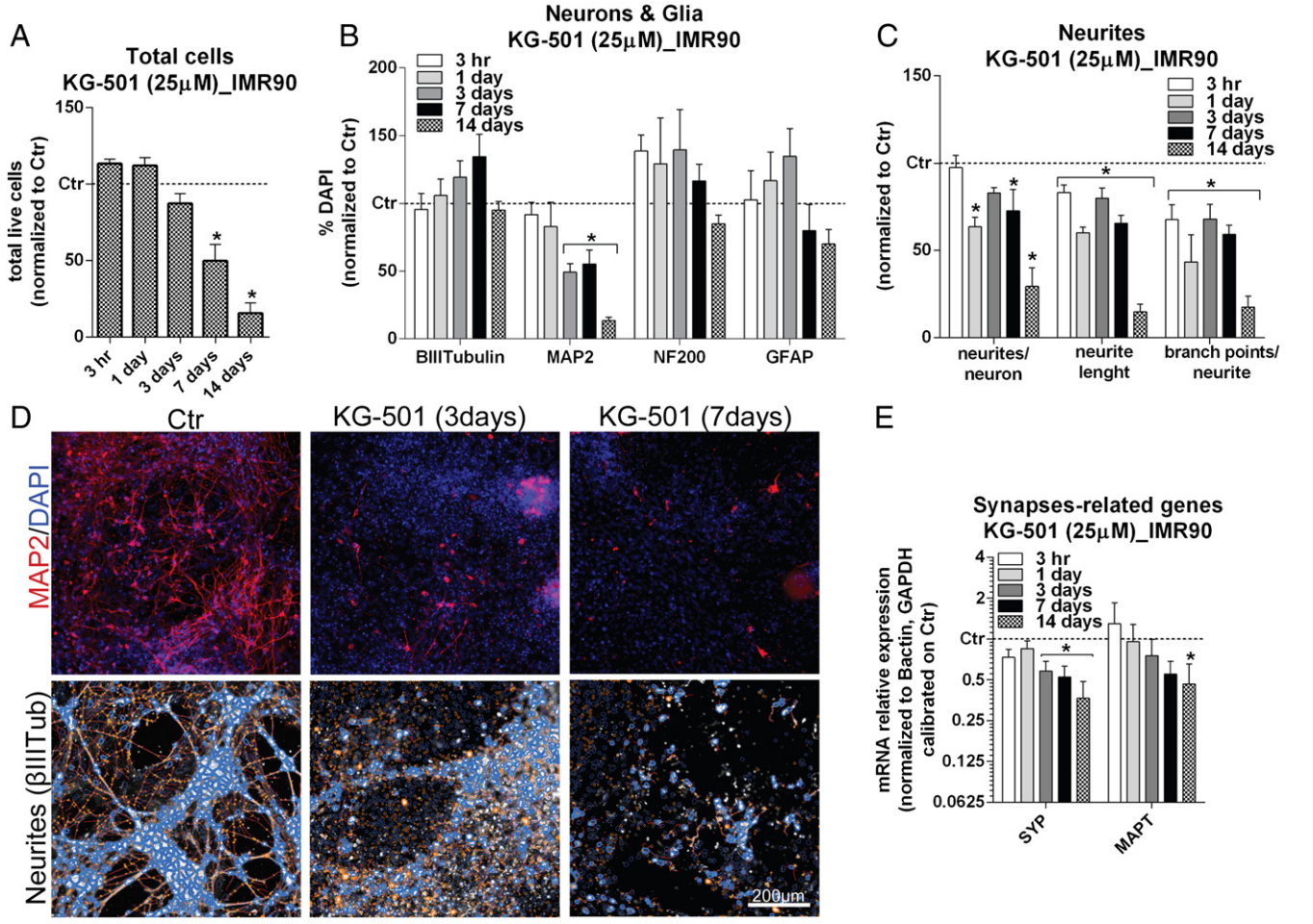

Fig. 5. Effects of KG-501 on selected endpoints in IMR90-derived neuronal cultures. (A–D) Analysis on the effect of a time-dependent 25 μM KG-501 exposure on total live cell number (i.e. non-pyknotic nuclei) (A), relative number of β-III-tubulin$^+$, MAP2$^+$, NF200$^+$ and GFAP$^+$ cells (B), neurite length, neurites/neuron and branch points/neurite (C) and representative immunocytochemical images of MAP2$^+$ cells (red, upper panels) and of neurites (black and white, β-III-tubulin stained cells, lower panels) comparing untreated cells (Ctr) and cells treated for 3 days and 7 days with 25 μM KG-501 (IMR90 p50) (D). (E) Effect of a time-dependent 25 μM KG-501 exposure on the expression of synaptogenesis-related genes (SYP and MAPT). Gene expression was normalized to β-actin and GAPDH and then calibrated to untreated cells (Ctr, dotted line, ΔΔCt method). For A–C, values were normalized to untreated cells (Ctr). For all the analyses, mean ± SEM of 3 analyses are shown.

3 days of KG-501 exposure (intermediate effects). These effects were followed by induction of cytotoxicity in the longer term (i.e. after 7 days), as shown by the overall reduction of cell viability (late effects) (Fig. 6). Notably, the early upregulation of both NR4A2 and FOS genes, might be related to the activation of pro-survival and/or stress response mechanisms within the cells, which could be a result of the inhibition of CREB. The upregulation of these genes has been reported in other studies describing the activation of NR4A2-Nurr1 in relation to oxidative stress (Sousa et al., 2007) and the upregulation of FOS caused by intermittent hypoxia (Nanduri and Nanduri, 2007) and by stimulant/anxiogenic drugs (Graybiel et al., 1990; Singewald et al., 2003). It should also be considered that the upregulation of these CREB-regulated genes upon KG-501 stimulation might also be evoked by CREB-independent mechanisms.

Importantly, the changes occurring within the first 3 days of exposure (i.e. reduction of BDNF-AS1 and SLC18A1 gene expression, decrease of MAP2+ cells and neurite-related measures) seem to be specific neuronal effects rather than preceding events of cytotoxicity, since we found that these exposures did neither show acute nor delayed effects on cell viability.

Altogether these data indicate that KG-501-induced inhibition of the CREB pathway can be related to cellular endpoints in our hiPSC-derived neuronal cultures which may be relevant for studying neurotoxicity. Among the analyzed endpoints, effects on neurite length and complexity and the reduction of MAP2$^+$ cell number showed to be the most sensitive and may represent relevant endpoints for neurotoxicity testing in vitro. Furthermore, considering the persistent downregulation of SLC18A1 and the time-dependent decrease of BDNF-AS1 expression, we hypothesize that SLC18A1 and BDNF-AS1 genes might represent sensitive markers to predict neurotoxic effects in vitro in relation to perturbations of the CREB pathway.

To further develop our test system and increase our understanding of the possible relation between CREB perturbation and chemical-induced cellular injury, the model should be challenged with a set of selected neurotoxic compounds. These follow-up studies should give insight on how often the CREB pathway is perturbed when the cells are exposed to neurotoxicants of diverse nature in order to assess the prevalence of CREB pathway perturbations for neurotoxicants and to assess whether measuring CREB pathway perturbations is useful for the prediction of neuronal cell injury. These studies may provide specific biomarkers related to pathway disturbance that can be measured at selected time points in order to predict whether new unknown compounds may cause neuronal cell injury. Moreover, further experiments with KG-501 and selected chemicals using neuronal cell cultures

derived from different hiPSC lines should be performed in order to assess possible inter-individual differences in toxicodynamics related to CREB pathway inhibition.

The hiPSC-based model may also be useful in activities related to the recently initiated adverse outcome pathway (AOP)-concept. An AOP is a conceptual framework that describes existing knowledge concerning the linkage between a molecular initiating event (MIE) and an adverse outcome (AO) that occurs at a level of biological organization relevant to risk assessment (Vinken, 2013). It consists of the description of key events that lead from the MIE to the AO (Vinken, 2013). At present, no AOP has been described in which perturbation of CREB signaling represents a key event in the AOP. Our cell model may be useful in the elucidation of a CREB-related AOP, and/or may be a relevant tool to measure effects on CREB signaling when AOPs would be developed that include CREB signaling perturbation as a key event.

The data on CREB signaling inhibition here presented indicate that this model can be used to study the relation of chemical-induced CREB pathway perturbation to chemical-induced (adverse) cellular effects. Further studies with well-known neurotoxicants may indicate whether perturbation of the CREB pathway may be relevant to screen for neurotoxicants, and as such qualify CREB pathway perturbation as a toxicity pathway.

Supplementary data to this article can be found online at http://dx.doi.org/10.1016/j.taap.2014.08.007.

Conflict of interest

The authors have no conflict of interest.

Acknowledgments

The authors are grateful to: the SCR&Tox neuronal working group (Dr. Giovanna Lazzari and Silvia Colleoni; both from Avantea srl, Cremona, Italy), Dr. Oliver Brüstle and Dr. Simone Haupt (both from the University of Bonn, Germany) for fruitful discussions, Dr. Elena Rampazzo and Luca Persano (University of Padova) for contributing to RPPA antibodies validation, Dr. Marc Peschansky and Dr. Mathilde Girard (I-stem) for providing IMR90-hiPSCs, Dr. Roman Liska (IHCP, JRC) for statistical analyses support and Dr. Anna Price (IHCP, JRC) for critical discussions. This work was supported by the EU-funded project "SCR&Tox" (Grant Agreement no. 266753) and DETECTIVE (Grant Agreement no. 266838).

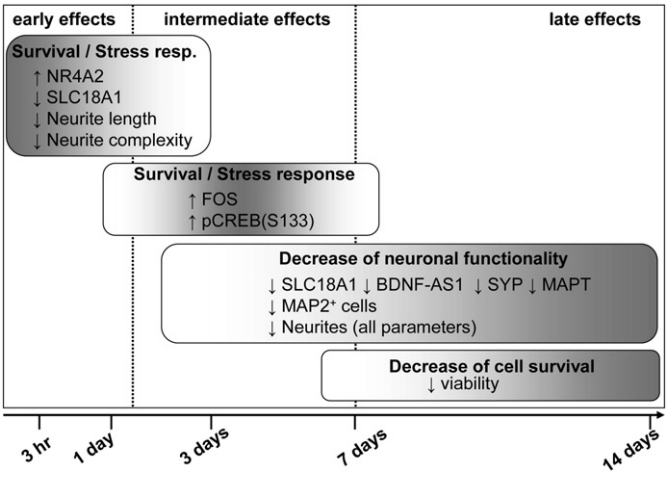

Fig. 6. Scheme summarizing the effects elicited by KG-501 on hiPSC-derived neuronal cultures. Upon inhibition of CREB signaling using KG-501, hiPSC-neurons activate pro-survival and/or stress-related responses, characterized by the immediate upregulation of NR4A2 gene and the downregulation of the vesicular neurotransmitter transporter-related gene SLC18A1 gene expression, occurring within 3 h, together with an impairment of neurite length and neurite complexity. A transient activation of CREB and upregulation of FOS gene occur within 1 day of KG-501 exposure (early effects). Furthermore, a progressive loss of neuronal functionality is observed, as shown by the sustained decrease of SLC18A1 gene, the time dependent downregulation of both BDNF-AS1 and SYP expression and the decrease of neurites and of $MAP2^+$ cells, occurring already after 3 days of KG-501 exposure (intermediate effects). After 7 days, KG-501 exposure elicits MAPT gene downregulation and overall reduction of cell viability (late effects).

References

NRC, National Research Council, 2007. Toxicity Testing in the 21st Century: A Vision and a Strategy. National Academy Press, Washington, DC, https://download.nap.edu/login.php?record_id=11970&page=%2Fdownload.php%3Frecord_id%3D11970.

Accordi, B., Espina, V., Giordan, M., VanMeter, A., Milani, G., Galla, L., Ruzzene, M., Sciro, M., Trentin, L., De Maria, R., te Kronnie, G., Petricoin, E., Liotta, L., Basso, G., 2010. Functional protein network activation mapping reveals new potential molecular drug targets for poor prognosis pediatric BCP-ALL. PLoS One 5, e13552.

Best, J.L., Amezcua, C.A., Mayr, B., Flechner, L., Murawsky, C.M., Emerson, B., Zor, T., Gardner, K.H., Montminy, M., 2004. Identification of small-molecule antagonists that inhibit an activator: coactivator interaction. Proc. Natl. Acad. Sci. U. S. A. 101, 17622–17627.

Bolstad, B.M., Irizarry, R.A., Astrand, M., Speed, T.P., 2003. A comparison of normalization methods for high density oligonucleotide array data based on variance and bias. Bioinformatics 19, 185–193.

Bruck, T., Benvenisty, N., 2011. Meta-analysis of the heterogeneity of X chromosome inactivation in human pluripotent stem cells. Stem Cell Res. 6, 187–193.

Brunelli, L., Llansola, M., Felipo, V., Campagna, R., Airoldi, L., De Paola, M., Fanelli, R., Mariani, A., Mazzoletti, M., Pastorelli, R., 2012. Insight into the neuroproteomics effects of the food-contaminant non-dioxin like polychlorinated biphenyls. J. Proteomics 75, 2417–2430.

Canovas-Jorda, D., Louisse, J., Pistollato, F., Zagoura, D., Bremer, S., 2014. Regenerative toxicology: the role of stem cells in the development of chronic toxicities. Expert Opin. Drug Metab. Toxicol. 10, 39–55.

Chalovich, E.M., Zhu, J.H., Caltagarone, J., Bowser, R., Chu, C.T., 2006. Functional repression of cAMP response element in 6-hydroxydopamine-treated neuronal cells. J. Biol. Chem. 281, 17870–17881.

Chandler, K.J., Barrier, M., Jeffay, S., Nichols, H.P., Kleinstreuer, N.C., Singh, A.V., Reif, D.M., Sipes, N.S., Judson, R.S., Dix, D.J., Kavlock, R., Hunter III, E.S., Knudsen, T.B., 2011. Evaluation of 309 environmental chemicals using a mouse embryonic stem cell adherent cell differentiation and cytotoxicity assay. PLoS One 6, e18540.

Damodaran, T.V., Gupta, R.P., Attia, M.K., Abou-Donia, M.B., 2009. DFP initiated early alterations of PKA/p-CREB pathway and differential persistence of beta-tubulin subtypes in the CNS of hens contributes to OPIDN. Toxicol. Appl. Pharmacol. 240, 132–142.

Daniels, B.R., Hale, C.M., Khatau, S.B., Kusuma, S., Dobrowsky, T.M., Gerecht, S., Wirtz, D., 2010. Differences in the microrheology of human embryonic stem cells and human induced pluripotent stem cells. Biophys. J. 99, 3563–3570.

Day, H.E., Kryskow, E.M., Nyhuis, T.J., Herlihy, L., Campeau, S., 2008. Conditioned fear inhibits c-fos mRNA expression in the central extended amygdala. Brain Res. 1229, 137–146.

Dix, D.J., Houck, K.A., Martin, M.T., Richard, A.M., Setzer, R.W., Kavlock, R.J., 2007. The ToxCast program for prioritizing toxicity testing of environmental chemicals. Toxicol. Sci. 95, 5–12.

Dragunow, M., Faull, R., 1989. The use of c-fos as a metabolic marker in neuronal pathway tracing. J. Neurosci. Methods 29, 261–265.

Drews, K., Jozefczuk, J., Prigione, A., Adjaye, J., 2012. Human induced pluripotent stem cells—from mechanisms to clinical applications. J. Mol. Med. (Berl.) 90, 735–745.

Eisen, M.B., Spellman, P.T., Brown, P.O., Botstein, D., 1998. Cluster analysis and display of genome-wide expression patterns. Proc. Natl. Acad. Sci. U. S. A. 95, 14863–14868.

Essand, M., Vikman, S., Grawe, J., Gedda, L., Hellberg, C., Oberg, K., Totterman, T.H., Giandomenico, V., 2005. Identification and characterization of a novel splicing variant of vesicular monoamine transporter 1. J. Mol. Endocrinol. 35, 489–501.

Gautier, L., Cope, L., Bolstad, B.M., Irizarry, R.A., 2004. affy—analysis of Affymetrix GeneChip data at the probe level. Bioinformatics 20, 307–315.

Ghosh, Z., Wilson, K.D., Wu, Y., Hu, S., Quertermous, T., Wu, J.C., 2010. Persistent donor cell gene expression among human induced pluripotent stem cells contributes to differences with human embryonic stem cells. PLoS One 5, e8975.

Ghosh, A., Manrique-Hoyos, N., Voigt, A., Schulz, J.B., Kreutzfeldt, M., Merkler, D., Simons, M., 2011. Targeted ablation of oligodendrocytes triggers axonal damage. PLoS One 6, e22735.

Graybiel, A.M., Moratalla, R., Robertson, H.A., 1990. Amphetamine and cocaine induce drug-specific activation of the c-fos gene in striosome-matrix compartments and limbic subdivisions of the striatum. Proc. Natl. Acad. Sci. U. S. A. 87, 6912–6916.

Ho, P.J., Yen, M.L., Yet, S.F., Yen, B.L., 2012. Current applications of human pluripotent stem cells: possibilities and challenges. Cell Transplant. 21, 801–814.

Judson, R.S., Houck, K.A., Kavlock, R.J., Knudsen, T.B., Martin, M.T., Mortensen, H.M., Reif, D.M., Rotroff, D.M., Shah, I., Richard, A.M., Dix, D.J., 2010. In vitro screening of environmental chemicals for targeted testing prioritization: the ToxCast project. Environ. Health Perspect. 118, 485–492.

Kleinstreuer, N.C., Judson, R.S., Reif, D.M., Sipes, N.S., Singh, A.V., Chandler, K.J., Dewoskin, R., Dix, D.J., Kavlock, R.J., Knudsen, T.B., 2011. Environmental impact on vascular development predicted by high-throughput screening. Environ. Health Perspect. 119, 1596–1603.

Krueger, W.H., Swanson, L.C., Tanasijevic, B., Rasmussen, T.P., 2010. Natural and artificial routes to pluripotency. Int. J. Dev. Biol. 54, 1545–1564.

Kumar, K.K., Aboud, A.A., Bowman, A.B., 2012. The potential of induced pluripotent stem cells as a translational model for neurotoxicological risk. Neurotoxicology 33, 518–529.

Lengner, C.J., Gimelbrant, A.A., Erwin, J.A., Cheng, A.W., Guenther, M.G., Welstead, G.G., Alagappan, R., Frampton, G.M., Xu, P., Muffat, J., Santagata, S., Powers, D., Barrett, C.B., Young, R.A., Lee, J.T., Jaenisch, R., Mitalipova, M., 2010. Derivation of pre-X inactivation human embryonic stem cells under physiological oxygen concentrations. Cell 141, 872–883.

Lister, R., Pelizzola, M., Kida, Y.S., Hawkins, R.D., Nery, J.R., Hon, G., Antosiewicz-Bourget, J., O'Malley, R., Castanon, R., Klugman, S., Downes, M., Yu, R., Stewart, R., Ren, B., Thomson, J.A., Evans, R.M., Ecker, J.R., 2011. Hotspots of aberrant epigenomic reprogramming in human induced pluripotent stem cells. Nature 471, 68–73.

Liu, X., Liu, W., Jin, Y., Yu, W., Liu, L., Yu, H., 2010. Effects of subchronic perfluorooctane sulfonate exposure of rats on calcium-dependent signaling molecules in the brain tissue. Arch. Toxicol. 84, 471–479.

Lonze, B.E., Ginty, D.D., 2002. Function and regulation of CREB family transcription factors in the nervous system. Neuron 35, 605–623.

Nanduri, J., Nanduri, R.P., 2007. Cellular mechanisms associated with intermittent hypoxia. Essays Biochem. 43, 91–104.

Numakawa, T., Suzuki, S., Kumamaru, E., Adachi, N., Richards, M., Kunugi, H., 2010. BDNF function and intracellular signaling in neurons. Histol. Histopathol. 25, 237–258.

O'Brien, P.J., Irwin, W., Diaz, D., Howard-Cofield, E., Krejsa, C.M., Slaughter, M.R., Gao, B., Kaludercic, N., Angeline, A., Bernardi, P., Brain, P., Hougham, C., 2006. High concordance of drug-induced human hepatotoxicity with in vitro cytotoxicity measured in a novel cell-based model using high content screening. Arch. Toxicol. 80, 580–604.

Osafune, K., Caron, L., Borowiak, M., Martinez, R.J., Fitz-Gerald, C.S., Sato, Y., Cowan, C.A., Chien, K.R., Melton, D.A., 2008. Marked differences in differentiation propensity among human embryonic stem cell lines. Nat. Biotechnol. 26, 313–315.

Pistollato, F., Bremer-Hoffmann, S., Healy, L., Young, L., Stacey, G., 2012. Standardization of pluripotent stem cell cultures for toxicity testing. Expert Opin. Drug Metab. Toxicol. 8, 239–257.

Radio, N.M., 2012. Neurite outgrowth assessment using high content analysis methodology. Methods Mol. Biol. 846, 247–260.

Rotroff, D.M., Dix, D.J., Houck, K.A., Knudsen, T.B., Martin, M.T., McLaurin, K.W., Reif, D.M., Crofton, K.M., Singh, A.V., Xia, M., Huang, R., Judson, R.S., 2013. Using in vitro high throughput screening assays to identify potential endocrine-disrupting chemicals. Environ. Health Perspect. 121, 7–14.

Sacchetti, P., Carpentier, R., Segard, P., Olive-Cren, C., Lefebvre, P., 2006. Multiple signaling pathways regulate the transcriptional activity of the orphan nuclear receptor NURR1. Nucleic Acids Res. 34, 5515–5527.

Saura, C.A., Valero, J., 2011. The role of CREB signaling in Alzheimer's disease and other cognitive disorders. Rev. Neurosci. 22, 153–169.

Schuh, R.A., Lein, P.J., Beckles, R.A., Jett, D.A., 2002. Noncholinesterase mechanisms of chlorpyrifos neurotoxicity: altered phosphorylation of Ca2+/cAMP response element binding protein in cultured neurons. Toxicol. Appl. Pharmacol. 182, 176–185.

Sell, S., 2010. On the stem cell origin of cancer. Am. J. Pathol. 176, 2584–2594.

Shamblott, M.J., Axelman, J., Littlefield, J.W., Blumenthal, P.D., Huggins, G.R., Cui, Y., Cheng, L., Gearhart, J.D., 2001. Human embryonic germ cell derivatives express a broad range of developmentally distinct markers and proliferate extensively in vitro. Proc. Natl. Acad. Sci. U. S. A. 98, 113–118.

Shaywitz, A.J., Greenberg, M.E., 1999. CREB: a stimulus-induced transcription factor activated by a diverse array of extracellular signals. Annu. Rev. Biochem. 68, 821–861.

Shen, Y., Matsuno, Y., Fouse, S.D., Rao, N., Root, S., Xu, R., Pellegrini, M., Riggs, A.D., Fan, G., 2008. X-inactivation in female human embryonic stem cells is in a nonrandom pattern and prone to epigenetic alterations. Proc. Natl. Acad. Sci. U. S. A. 105, 4709–4714.

Silva, S.S., Rowntree, R.K., Mekhoubad, S., Lee, J.T., 2008. X-chromosome inactivation and epigenetic fluidity in human embryonic stem cells. Proc. Natl. Acad. Sci. U. S. A. 105, 4820–4825.

Singewald, N., Salchner, P., Sharp, T., 2003. Induction of c-Fos expression in specific areas of the fear circuitry in rat forebrain by anxiogenic drugs. Biol. Psychiatry 53, 275–283.

Sipes, N.S., Martin, M.T., Reif, D.M., Kleinstreuer, N.C., Judson, R.S., Singh, A.V., Chandler, K.J., Dix, D.J., Kavlock, R.J., Knudsen, T.B., 2011. Predictive models of prenatal developmental toxicity from ToxCast high-throughput screening data. Toxicol. Sci. 124, 109–127.

Smyth, G.K., 2004. Linear models and empirical Bayes methods for assessing differential expression in microarray experiments. Stat. Appl. Genet. Mol. Biol. 3 (Article3).

Sousa, K.M., Mira, H., Hall, A.C., Jansson-Sjostrand, L., Kusakabe, M., Arenas, E., 2007. Microarray analyses support a role for Nurr1 in resistance to oxidative stress and neuronal differentiation in neural stem cells. Stem Cells 25, 511–519.

Stummann, T.C., Hareng, L., Bremer, S., 2009. Hazard assessment of methylmercury toxicity to neuronal induction in embryogenesis using human embryonic stem cells. Toxicology 257, 117–126.

Tchieu, J., Kuoy, E., Chin, M.H., Trinh, H., Patterson, M., Sherman, S.P., Aimiuwu, O., Lindgren, A., Hakimian, S., Zack, J.A., Clark, A.T., Pyle, A.D., Lowry, W.E., Plath, K., 2010. Female human iPSCs retain an inactive X chromosome. Cell Stem Cell 7, 329–342.

Trosko, J.E., Chang, C.C., 2010. Factors to consider in the use of stem cells for pharmaceutic drug development and for chemical safety assessment. Toxicology 270, 18–34.

VanElzakker, M., Fevurly, R.D., Breindel, T., Spencer, R.L., 2008. Environmental novelty is associated with a selective increase in Fos expression in the output elements of the hippocampal formation and the perirhinal cortex. Learn. Mem. 15, 899–908.

Vinken, M., 2013. The adverse outcome pathway concept: a pragmatic tool in toxicology. Toxicology 312, 158–165.

Wu, Z., Puigserver, P., Andersson, U., Zhang, C., Adelmant, G., Mootha, V., Troy, A., Cinti, S., Lowell, B., Scarpulla, R.C., Spiegelman, B.M., 1999. Mechanisms controlling mitochondrial biogenesis and respiration through the thermogenic coactivator PGC-1. Cell 98, 115–124.

Xu, Y., Zhang, C., Wang, R., Govindarajan, S.S., Barish, P.A., Vernon, M.M., Fu, C., Acharya, A.P., Chen, L., Boykin, E., Yu, J., Pan, J., O'Donnell, J.M., Ogle, W.O., 2011. Corticosterone induced morphological changes of hippocampal and amygdaloid cell lines are dependent on 5-HT7 receptor related signal pathway. Neuroscience 182, 71–81.

Yamamoto, H., Demura, T., Morita, M., Banker, G.A., Tanii, T., Nakamura, S., 2012. Differential neurite outgrowth is required for axon specification by cultured hippocampal neurons. J. Neurochem. 123, 904–910.

Zuo, Z., Cai, J., Wang, X., Li, B., Wang, C., Chen, Y., 2009. Acute administration of tributyltin and trimethyltin modulate glutamate and N-methyl-D-aspartate receptor signaling pathway in *Sebastiscus marmoratus*. Aquat. Toxicol. 92, 44–49.